Fibre-Reinforced Geopolymers (FRGPs) as inorganic composites for flexural strengthening of brick masonry

Enrico Garbin[a]*, Matteo Panizza[b], Marco Natali[c], Gilberto Artioli[d], and Sergio Tamburini[e]

[a] National Research Council of Italy (CNR), Institute of Condensed Matter Chemistry and Technologies for Energy (ICMATE), Corso Stati Uniti 4, 35127, Padova, Italy. ORCID: 0000-0003-3276-7444 email: enrico.garbin@cnr.it

* *corresponding author*

[b] National Research Council of Italy (CNR), Institute of Condensed Matter Chemistry and Technologies for Energy (ICMATE), Corso Stati Uniti 4, 35127, Padova, Italy. ORCID: 0000-0003-0259-3914 email: matteo.panizza@cnr.it

[c] National Research Council of Italy (CNR), Institute of Condensed Matter Chemistry and Technologies for Energy (ICMATE), Corso Stati Uniti 4, 35127, Padova, Italy. email: marcostefano.natali@cnr.it

[d] University of Padua, Dept. of Geosciences, Via G. Gradenigo 6, 35131 Padova, Italy. ORCID: 0000-0002-8693-7392 email: gilberto.artioli@unipd.it

[e] National Research Council of Italy (CNR), Institute of Condensed Matter Chemistry and Technologies for Energy (ICMATE), Corso Stati Uniti 4, 35127, Padova, Italy. Email: sergio.tamburini@cnr.it

Authors' biographical notes

Enrico Garbin. M.Sc. in Architectural Engineering and Ph.D. in Design, Preservation and Control of Materials and Structures. Currently researcher at the National Research Council of Italy – CNR, ICMATE Institute. Formerly postdoctoral at the CIRCe Centre of the University of Padova. Lecturer of the Advanced M.Sc. in Structural Analysis of Monuments and Historical Constructions. Associate Editor of the Journal of Cultural Heritage. His current research activities are in mechanical-physical characterization of innovative cementitious materials and structural design of related applications and products.

Matteo Panizza. M.Sc. in Architectural Engineering and Ph.D. in Study and Preservation of Archeological and Architectural Heritage. Currently researcher at the National Research Council of Italy – CNR, ICMATE Institute. Formerly focused on strengthening techniques for existing buildings, his research activities currently involve mechanical-physical characterization of innovative binders and construction materials, use of recycled aggregates and design of sustainable and energy efficient architectural components.

Marco Natali. M.Sc. and Ph.D. in Physics. Post-doctoral at LPN-CNRS in Paris, France, then researcher at the National Research Council of Italy – CNR, ICMATE Institute. His research activities involve: III-V semiconductor hetero-structures; X-ray diffraction; magnetic nanostructures; nano-imprint lithography; microfluidics and environmental trace metal analysis; geopolymers and innovative binders.

Gilberto Artioli. M.Sc. in Geological Sciences (University of Modena, IT) and Ph.D. in Geophysical Sciences (University of Chicago, USA). Presently full professor at the University of Padua, Italy, and former director of the CIRCe Centre for the investigation of cement materials. His main research interests involve materials science, mineralogy and crystallography, archaeometry and archaeological science.

Sergio Tamburini. Ms.C. in Chemistry, former senior scientist and currently associate at the National Research Council of Italy – CNR, ICMATE Institute. His research activities deal with basic and applied research in chemistry, nano and supramolecular chemistry, materials science, science and technology for development of Alkali Activated Materials (AAM), including Geopolymeric materials.

Fibre-Reinforced Geopolymers (FRGPs) as inorganic composites for flexural strengthening of brick masonry

Enrico Garbin*, Matteo Panizza, Marco Natali, Gilberto Artioli, and Sergio Tamburini

Abstract

This study presents an assessment of externally bonded Fibre-Reinforced GeoPolymers (FRGPs) as strengthening material for masonry structures. Geopolymer matrices can also potentially fulfil the requirements of restoration criteria for historical buildings, with heat-resistant performances generally better than Fibre-Reinforced Polymers (FRPs). Four FRGPs, including either unidirectional steel or bidirectional carbon, basalt or glass mesh as reinforcement, were tested by means of local shear and bending tests on fired clay brick specimens, either alone or coupled with hydraulic lime mortar. In addition, the behaviour of each reinforcement exposed to alkaline environments was investigated through tensile tests on coupons. Results confirmed the interesting potential of FRGPs for strengthening masonry elements, highlighting a good performance of steel and carbon reinforcements.

Keywords

Geopolymers; Alkali-Activated Materials (AAM); Fibre Reinforced Geopolymers; FRCM; TRM; Composite Materials; Strengthening; Masonry structures.

1. Introduction

Existing masonry buildings and Built Heritage (BH) require a permanent maintenance process to withstand the effects of hazardous natural events and mitigate their effects. This can be accomplished by devoted activities of restoration and structural repair adopting traditional and innovative materials and intervention techniques (Modena et al. 2011; Tomaževič 2011; Valluzzi, Modena, and de Felice 2014). In the last three decades, the use of Externally Bonded Fibre Reinforced Polymers (EB-FRPs) has grown to be one of the reference interventions for existing buildings and for BH (Triantafillou 1998; Shrive 2006; Garbin, Panizza, and Valluzzi

2018). The main advantages of EB-FRPs that fostered their widespread application on existing structures, including also those belonging to the BH, are for instance: their ease and flexibility of application, their fast curing and the related ability in carrying tensile stresses in few hours or days, low weight in comparison to many traditional materials (e.g. steel rods/plates), the high tensile strength and stiffness-to-weight ratio, enhanced fatigue and endurance in aggressive environments (Valluzzi, Modena, and de Felice 2014; Shrive 2006; Hollaway 2010). Nevertheless, FRPs have some compatibility and removability issues with existing and BH masonry structures, mainly due to the adoption of organic matrices (Valluzzi, Modena, and de Felice 2014; Tedeschi et al. 2014). In the last couple of decade, the replacement of organic matrices (e.g. epoxy) with inorganic cement or lime-based mortars has been investigated (Papanicolaou et al. 2007; Papanicolaou et al. 2008; Garmendìa et al. 2014; de Felice et al. 2014; Kouris and Triantafillou 2018). The combination of fibres, usually in the form of meshes, with inorganic matrices is currently often labelled with the acronym of Fibre Reinforced Cementitious Matrix (FRCM) (American Concrete Institute [ACI] 2013; National Research Council of Italy [CNR] 2020), acronym that also covers for cement-free binders, while in several former publications the acronym Textile Reinforced Mortars (TRM) was used (Valluzzi, Modena, and de Felice 2014; de Felice 2014; Kouris and Triantafillou 2018). Advantages of FRCMs over FRPs include: better compatibility with masonry substrates and traditional craftsmanship, reversibility, better behaviour under high temperatures and lack of toxic vapours in case of fire, resistance to Ultra-Violet (UV) radiation, water vapour permeability, applicability over moist substrates, greater deformability and potential lower cost (Valluzzi, Modena, and de Felice 2014; Garbin, Panizza, and Valluzzi 2018; Tedeschi et al. 2014; de Felice et al. 2014; Kouris and Triantafillou 2018). Moreover, inorganic matrices appear particularly suitable for applications to masonry structures, where the bond strength of epoxy matrices can hardly be entirely used due to the inherent mechanical characteristics of the

substrate, and for a better compliance with restoration criteria, especially when cement-free matrices are adopted (Valluzzi, Modena, and de Felice 2014; Garbin, Panizza, and Valluzzi 2018; de Felice et al. 2014; Kouris and Triantafillou 2018). Nevertheless, traditional lime based inorganic mortars compatible with BH often show low adhesion to masonry substrates and between the FRCM layers (Valluzzi, Modena, and de Felice 2014; Garbin, Panizza, and Valluzzi 2018; Kouris and Triantafillou 2018). To overcome this issue, geopolymers were studied as possible efficient and compatible inorganic matrices for existing masonry substrates and BH (Tamburini et al. 2017; Gkournelos, Azdejković, and Triantafillou 2022). Indeed, geopolymer can meet the dedicated restoration requirements of BH, thanks to their typical chemical composition and porosity which are similar to that of clay bricks (Tamburini et al. 2017), while delivering physical-mechanical performances exceeding those of the best inorganic matrices used in FRCMs (Tamburini et al. 2017; Provis and van Deventer 2009).

Geopolymers are relatively recent and emerging inorganic cement-free binders that present a combination of the best characteristics of ceramic and cement-based materials (Tamburini et al. 2017; Provis and van Deventer 2009). Moreover, they have a clear advantage over EB FRPs and FRCMs as non-flammable and heat-resistant matrices for inorganic composites designed to reach temperatures of 1000°C (Tamburini et al. 2017; Kurz and Balaguru 2001). Geopolymers are inorganic quasi-fragile materials produced from aluminosilicates typically activated with alkali hydroxide and/or alkali silicate solutions. Several aluminosilicate or calcium-aluminosilicate raw materials can be used, such as dehydroxylated aluminosilicate clay mineral (e.g. metakaolin) and industrial by-products resulting from high temperature processes such as fly ash or ground blast furnace slag, among others (Provis and van Deventer 2018). They are also materials suitable for a greener economy, since they can be derived from by-products or from the recycling of industrial waste materials, and they can be produced with up to ten times lower CO_2 emission than Portland cement (Provis and van Deventer 2018; Pacheco-

Torgal and Jalali 2011). Geopolymer grouts and mortars can be obtained by charging the geopolymer binder with sand or fine aggregates (Tamburini et al. 2017; Provis and van Deventer 2009).

Fibre Reinforced GeoPolymer (FRGP) is the combination of a geopolymer grout with fibre meshes or fabrics, similarly to Fibre Reinforced Cement Mortars (FRCM) (Tamburini et al. 2017). Several studies were done on geopolymer fibre composites as final product made with both short fibres (Shaik 2013; Welter, Schmücker, and MacKenzie 2014; Vickers, van Riessen, and Rickard 2015) and multiple laminated layers of fabrics (Kurz and Balaguru 2001; Toutanji and Deng 2007; Ferone et al. 2013), fewer investigations exist on FRGPs for retrofitting structural elements, and most investigations focused on strengthening Reinforced Concrete (RC) beams (Papakonstantinou and Katakalos 2009; Menna et al. 2013; Katakalos and Papakonstantinou 2009; Carabba et al. 2017). Whereas, little contributions on the use of FRGPs as strengthening materials for existing masonry structures are present (Tamburini et al. 2017; Gkournelos, Azdejković, and Triantafillou 2022; Garbin et al. 2014). Indeed, FRGPs are inorganic polymeric matrices with a quasi-fragile behaviour (Tamburini et al. 2017; Provis and van Deventer 2009; Garbin et al. 2014). Consequently, the mechanical models and the design procedures available for FRCMs (American Concrete Institute [ACI] 2013; National Research Council of Italy [CNR] 2020; Ceroni and Salzano 2018; Meriggi, de Felice and De Santis 2020) can be adopted. Lastly, for a successful application of FRPs, their durability should be evaluated. Geopolymers have already shown good resistance towards acid and alkaline environments (Tamburini et al. 2017; Provis and van Deventer 2009). Therefore, the main durability issue is connected to the endurance of the fibres when embedded in a geopolymeric matrix, which provide an alkaline environment that might result corrosive for certain reinforcements as glass or basalt fibres (Gkournelos, Azdejković, and Triantafillou 2022; Tamburini et al. 2015; Dhand et al. 2015). Indeed, this is a common issue for the glass fibre

laths embedded in lime or cement plasters and for any fibre mesh embedded in the cementitious matrices of FRCMs (Triantafillou 2016).

2. Research scope

The experimental research aims at promoting the yet untapped and interesting potential of FRGPs as strengthening materials for masonry elements (Tamburini et al. 2017; Gkournelos, Azdejković, and Triantafillou 2022). In this framework, the behaviour of 4 Fibre Reinforced GeoPolymers (FRGPs) was explored by means of local tests on masonry units and sub-assemblages made of soft-mud clay bricks bound by hydraulic lime mortar. FRGPs embedded either a unidirectional Ultra High Strength Steel (UHSS) fabric or a bi-directional mesh of non-metallic fibres, either carbon, basalt, or alkali-resistant glass, respectively. The behaviour of each reinforcement in alkaline environments was studied through tensile tests on coupons immersed for 28 days in 4 alkaline solutions, tentatively simulating the pore solution of the geopolymeric matrices. Bond and flexural performances of FRGPs were explored via single lap shear tests on single bricks, with a bonded length of either 200 or 50 mm, and via 3-point bending tests on specimens reinforced at the bottom face. Bending specimens were made of either one or two slices of soft mud bricks, in the latter case longitudinally connected by a mortar joint. Specimens with FRGPs were tested at more than 3 months of age, so that the geopolymer matrix can be assumed to have achieved its final strength, as per Figure 9 in Tamburini et al. (2017).

3. Materials and methods

3.1. Materials

3.1.1. Bricks and mortar

Low-strength soft mud clay bricks were used with the intent of simulating typical historical masonry units (Coletti et al, 2016). Their nominal sizes were 250 × 120 × 55 mm³, and facing

surfaces were not sandy, contrarily to most similar products commonly available. They were the same type of bricks tested in Tamburini et al. (2017), although coming from a different batch used in Girardello's thesis (2013). The mortar forming the joint in 2-brick flexural specimens was a commercially available pre-mixed cement-free pozzolana lime mortar with siliceous sand aggregates, category M15 according to Eurocode 6 (European Committee for Standardization 2005). The measured properties of bricks (strengths found in Girardello 2013, elastic modulus in Panizza et al. 2012) and mortar (strengths and elastic modulus from Garbin 2008) are listed in Table 1, where ρ_{app} stands for apparent density, *OP* for open porosity measured via the buoyancy method, E_c for elastic modulus in compression, and f_c, f_b and f_{sp} indicate compressive, bending and splitting strengths, respectively.

[/t]Table 1 near here[/t]

The FRGP matrix was a geopolymer grout, extensively described in Tamburini et al. (2017), prepared with metakaolin (MK) and ground granulated furnace slag (SL) as solid precursors, and sodium silicate (Na-Sil), with molar ratio SiO_2/Na_2O ~ 1.5 and concentration of 41.3%, as liquid activator. The binder embedded fine siliceous sand (grain size of 0.1–0.7 mm) and wollastonite (grain size of 0.05–0.45 mm) in 1:2 proportion as inorganic aggregates, added to achieve a MK:SL:aggregate weight ratio of 1:2:4. Based on the chemical composition of reagents, the binder had the following nominal molar ratios: Si/Al ≈ 2.18, Na/Si ≈ 0.37 and Na/Al ≈ 0.82.

The measured physical and mechanical properties are listed in Table 2, where ρ_{app} and *OP* indicate apparent density and open porosity measured via buoyancy method; $f_{c,28d}$, $f_{b,28d}$ and f_{sp} are compressive, bending and splitting strengths at 28 days of age, and E_c is the elastic modulus in compression. Each parameter was tested on at least 3 samples. Long term tests substantially confirmed the stability of strength, since f_c measured at 3 months, 1 year and 3.5 years of age

delivered mean values of 43.7 (CoV 6.5%), 46.4 (1.7%) and 44.6 (3.0%) N/mm², respectively, while f_b at 3 months was 7.4 N/mm² (14.1%) in average.

[t]Table 2. near here[/t]

3.1.2. Epoxy resin

A bi-component epoxy resin, available as part of a commercial FRP system, was used to impregnate fibres for tensile coupons and for bending specimens made of single bricks reinforced at their bottom. The resin was tested in direct tension by means of 12 dog-bone specimens (length × width × thickness 215 × 13 × 4 mm³) in a universal test frame equipped with a 25 kN load cell and a PLAST extensometer having a 25 mm gauge length, as done in Valluzzi et al. (2012). The measured average tensile strength was 32.9 N/mm² (CoV 9.6%), which delivered a characteristic (5-percentile) value of 27.0 N/mm². The average strain at maximum load was 3.8% (CoV 6.0%). The average elastic moduli were $1.88 \cdot 10^3$ (CoV 21.5%) and $1.34 \cdot 10^3$ N/mm² (CoV 14.5%), calculated between 10–40% and 30–60% of the maximum load, respectively.

3.1.3. Fibre reinforcements

The geopolymer matrix was coupled with 4 types of fibre reinforcements, either a unidirectional steel fabric or three types of bidirectional fibre mesh, i.e. carbon, basalt or glass, thus generating 4 Fibre-Reinforced GeoPolymers (FRGPs). The main properties of steel fabric and non-metallic meshes are listed in Table 3, where ρ_s is the surface density, t_{ef} is the equivalent dry thickness, E is the Young's modulus in tension, f_t is the tensile strength, and the subscripts *ds*, *exp*, and *cal* indicate quantities from technical datasheets, experimentally measured or calculated, respectively.

The unidirectional steel fabric (STL) was composed by ultra-high tensile strength steel cords, each consisting of 3 straight and 2 twisted coated wires, mounted on a thin plastic mesh by means of thermoplastic resin and about 6 mm spaced apart (low-density fabric). The datasheet

reported a characteristic tensile strength of 3070 N/mm², an average elastic modulus of $190 \cdot 10^3$ N/mm² and an equivalent thickness of 0.075 mm, being the area of a single cord equal to 0.538 mm².

The carbon reinforcement (CAR) was a bidirectional balanced mesh made of uncoated strands with a centre-to-centre spacing of about 9.3 mm in both direction (Garbin, Panizza, and Valluzzi 2018). According to its technical datasheet, it has a surface density of 200 g/m², a characteristic tensile strength of 2500 N/mm², an average elastic modulus of $230 \cdot 10^3$ N/mm² and an equivalent thickness of 0.048 mm. Being the equivalent thickness not disclosed at the time, a reversed calculation carried out by Garbin et al. (2018) delivered a value of 0.056 mm, which was herein used in the analyses because the material belonged to the same supply.

The basalt reinforcement (BAS) was a bidirectional balanced mesh made of uncoated strands with a centre-to-centre spacing of about 8.0 mm, with a declared surface density of 300 g/m². As reported in the technical datasheet, it has a characteristic tensile strength of 1735 N/mm², an average elastic modulus of $90 \cdot 10^3$ N/mm² and an equivalent thickness of 0.053 mm.

Lastly, the glass reinforcement (ARG) was a bidirectional balanced mesh made of uncoated strands of alkali-resistant glass. Although balanced, it presents strands spaced about 7.7 mm in the weft direction and about 6.7 mm along the warp, so that the area of a single element is different according to its direction (Garbin, Panizza, and Valluzzi 2018). The current technical datasheet declares a surface density of 240 g/m², a characteristic tensile strength of 1300 N/mm², an average elastic modulus of $65 \cdot 10^3$ N/mm² and an equivalent thickness of 0.036 mm. Nonetheless, the datasheet available at the time of the supply reported a surface density of 220 g/m², the other properties being the same. Hence, as for carbon, a reversed calculation was carried out (Garbin, Panizza, and Valluzzi 2018), which delivered a value of 0.042 mm for the equivalent thickness.

[t]Table 3 near here[/t]

3.2. Test methods

The experiments, detailed in the following, consisted in:

- tensile tests on fibre coupons (all reinforcements and 4 conditioning types, 4 to 9 repetitions per each combination);
- shear tests on reinforcements applied to single bricks with either 200 mm (all reinforcements but glass fibres, 3 repetitions), or 50 mm of bonded length (steel and basalt fibres only, 2 repetitions);
- 3-point bending tests on single-brick slices, either unreinforced, reinforced with the geopolymer matrix only (without fibres), or reinforced with fibres (all reinforcements) embedded either in geopolymer or epoxy matrix (3 repetitions);
- 3-point bending tests of 2-brick slice specimens with a mortar joint, reinforced with fibres embedded in geopolymer matrix (all reinforcements but glass fibres, 3 repetitions).

3.2.1. Tensile tests on fibre coupons

Either single cords, in the case of steel fibres, or 2-strand coupons, in the case of carbon, basalt and glass fibres, were tested in tension in a 25 kN electro-mechanic universal machine. Specimens were 380 mm long to allow a free length of about 280 mm after gluing with epoxy resin 2 aluminium tabs 50 mm long, or sleeves in case of cords, at each end for a proper clamping to the test machine (Fig. 1). Carbon, glass, and basalt strands were impregnated with a small amount of epoxy resin for preventing or limiting possible uneven distribution of stresses inside the reinforcement, thus closely measuring the resistance of the mesh. The width of test coupons - epoxy included - was approximately comprised between 14 and 19 mm according to the type of mesh, although these values were not included in calculations that were based on strands' area.

Tests were carried out on either pristine samples of reinforcements (C0 condition) or fibres immersed for 28 days in 4 alkaline solutions to investigate their possible degradation in alkaline environments, as those of the geopolymer matrices. C1 consisted in a 5% aqueous solution of NaOH (corresponding to 1.25M), according to the standard ASTM E2098/E2098M (ASTM International 2013). Aqueous solutions of either sodium (the same used as binder activator) or potassium silicate were adopted for C2 and C3, respectively. The formulation of potassium and sodium silicates had the same molar ratio SiO_2/M_2O ~ 1.5, with a solid matter concentration of 46.0%. Silicates were dissolved in water to achieve the same concentration of Na (or K) ions of the C1 solution. C4 corresponded to a solution of sodium silicate with a concentration 4 times higher than C2. After the immersion, fibres were rinsed and dried to measure the weight loss by means of an analytical scale (Sartorius GC803S, accuracy class I, scale interval $2 \cdot 10^{-4}$ g). Four to 9 tensile coupons were tested per each type of reinforcement and conditioning solution.

[f]Figure 1 near here[/f]

3.2.2. Single-lap shear tests

Specimens consisted in a single brick with the FRGP applied longitudinally onto the wider surface (Fig. 2a) with a bonded area 200 mm long and 60 mm wide, carefully delimited by masking tape. A protruding portion extending for about 220 mm beyond the edge of the brick was used for the connection to the test machine. The reinforcement was embedded inside the geopolymer matrix for the whole length, except in the case of steel cords that were kept bare beyond the edge of the brick. The area of the reinforcement varied according to the type, since the FRGP included either 8 steel cords, 5 carbon or 7 basalt strands to achieve the desired width. The test setup (Fig. 2b), designed for a universal electro-mechanic machine, was the same already adopted in several former researches, e.g. Panizza et al. (2012) and Garbin, Panizza, and Valluzzi (2018). It consisted in two steel plates 50 mm thick connected by 4 threaded bars with diameter of 16 mm, two of which fastened to the bottom head of the test machine. The

specimen was inserted between those plates, taking care about alignments and contacts, and gluing the protruding reinforcement with a quick setting resin to a steel part connected to the upper loading head of the test machine by means of a ball joint. Four potentiometers were used to monitor displacements, two positioned at the beginning of the 200 mm bonded length (L_b), one in the middle and one at the unloaded end of the FRGP. Tests were carried out in displacement control, with a rate of the movable transverse beam progressively incremented from 0.3 mm/min to 1.2 mm/min. Load and displacement values were recorded by an external acquisition system at 10 Hz.

Three specimens per type of reinforcement were tested, for overall 9 samples. Two specimens with steel and 2 with basalt FRGP were re-tested with a bonded length of 50 mm (Fig. 2c), after carefully cutting and removing the exceeding portion of brick. In this case, only 2 potentiometers, positioned at the beginning of the 50 mm bonded length, were used.

[f]Figure 2 near here[/f]

3.2.3. 3-point bending tests on 1-brick and 2-brick reinforced specimens

Three-point bending tests were carried out on brick slices about 32 mm wide, either single or longitudinally aligned two by two and connected by a 10 mm mortar joint (Fig 3a), thus obtaining samples approximately 510 mm long. The choice of thin specimens was aimed at limiting possible uneven stress distributions across the width of the FRGP reinforcement.

The FRGP was centrally applied to the bottom side, extending for about 170 mm, in single-slice specimen, or 330 mm. It has to be noted that, in single-slice specimens, the reinforcing fibres ended before the support line, while the geopolymer matrix was extended to the edge of the substrate to allow for an easier casting. The reinforcement comprised 3 cords or strands for each type of fibre. FRP reinforcements, i.e. the same fibres embedded in epoxy resin, were applied to additional single-slice specimens.

A 50 kN electro-mechanic universal machine, equipped with a commercial setup for bending (Fig. 3b), was used. The span between bottom supports was either 200 mm (single-slice specimens) or 380 mm, slightly greater than the length of the FRGP. Contacts between sample and steel supports were improved by small rubber pads. Tests were carried out in displacement control, with a rate of the loading beam of either 0.15 mm/min (single-slice specimens) or 0.5 mm/min. Load and displacements were recorded by the embedded acquisition system of the universal machine.

Three specimens per type of reinforcement were tested, for overall 24 single-slice and 9 2-slice samples. The strength of 3 single brick slice samples with the geopolymer matrix applied without fibres, and 3 2-slice unreinforced specimens, was measured as reference. The latter samples were tested twice at 0.1 mm/min with a 2.5 kN load cell, repairing the failed joint with epoxy resin and testing again the same specimen to also measure the resistance of the strongest mortar-brick interface.

[f]Figure 3 near here[/f]

4. Experimental results and discussion

4.1. Tensile tests on conditioned fibre reinforcements

Failure was generally as expected, with a fibre tensile rupture located inside the free length between the anchoring, in some cases close to the tabs. Although few specimens showed an irregular failure, due to slippage problems at the clamping with the test machine or to an imperfect alignment, at least 4 suitable results per test combination were included in the calculations. As a general reference, pH measured values of alkali solutions and 2 batches of the hardened geopolymer matrix are reported in Table 4.

Average ($f_{t,avg}$) and characteristic ($f_{t,k}$) – i.e. 5-percentile – tensile strengths calculated from the recorded maximum load and grouped by fibre and conditioning type, are listed in Table 5

together with their Coefficient of Variation (CoV). Measured values of weight loss are shown in Figure 4a, whereas tensile strength retentions are shown in Figure 4b.

Steel cords were substantially not affected by the alkaline environment, with a measured strength loss always lower than 3%, reasonably included within a common experimental variability, despite a weight loss that exceeded 3% in two cases. Carbon fibres showed a strength retention of about 93% in sodium hydroxide and sodium silicate solutions, and were slightly more sensitive to potassium silicate solutions, with a lower strength retention (86%). Conversely, they showed the lowest values of weight loss (about 0.2–0.3%). Finally, as expected, the uncoated basalt fibres showed the worst degradation, with a strength loss of about 25% in silicate solutions and 45% in sodium hydroxide solution, and a weight loss comprised between 0.7 to 1.9% (the lowest measured in NaOH). Strength conversion coefficients for aggressive environments proposed by the Italian guidelines CNR DT200R1 (National Research Council of Italy [CNR] 2013) – 0.85 for carbon and 0.50 for glass fibres – and CNR DT215 (National Research Council of Italy [CNR] 2020) – 0.70 regardless of the fibres type, compared to the present experimental results (Tab. 6), appear reasonably close where applicable. The experimental results shown no apparent correlation between weight loss and strength retention. As also underlined by Gkournelos, Azdejković, and Triantafillou (2022), the type of fibre's sizing plays a key role in the fibre mesh durability. In fact, our uncoated basalt reinforcement showed marked reductions of the strength retention factors, whereas the alkali resistant glass reinforcement presented strength retention factors similar to those of the more durable carbon reinforcement. Lastly, it is worth recalling that reinforcements with less statistically dispersed results provided better characteristic tensile strengths, which are those used within design calculations, therefore it might occur that lower average values correspond to greater characteristic strengths.

[t]Table 4 near here[/t]

[t]Table 5 near here[/t]

[f]Figure 4 near here[/f]

[t]Table 6 near here[/t]

4.2. Single-lap shear tests

Failures were substantially different for each type of FRGP. Steel cords broke in tension in 2 specimens (Fig. 5a), while in one case a partial debonding occurred with the detachment of about 2/3 of the bonded length (Fig. 5b). Carbon strands caused a diffuse cracking of the matrix (Fig. 5c) and generally slipped inside the geopolymer (Fig. 5d), with minor signs of tensile failure in the most external fibrils that are likely those partially embedded in the geopolymeric matrix, as also reported in Zhu et al. (2021), and several cracks in the free protruding FRGP, which were about 25-30 mm spaced. On the other hand, basalt strands showed a rather clear tensile rupture without noticeable signs of slippage, for both 200 (Fig. 6a) and 50 mm (Fig. 6b) of bonded length, whereas 50 mm steel FRGP specimens induced a cohesive debonding failure inside the brick, tearing off a portion about 1 cm deep (Fig. 6c).

[f]Figure 5 near here[/f]

[f]Figure 6 near here[/f]

The recorded load–loaded end displacement curves are reported in Figure 7, both compared together and shown separately, to take into consideration the different orders of magnitude of forces and displacements related to the various reinforcements. Results, in terms of failure mode, maximum load P_{max} and maximum stress σ_{max} (load and fibres area ratio), are listed in Table 7, together with the exploitation coefficient η_{ST} calculated as the ratio of σ_{max} and the fibre tensile strength $f_{t,avg}$ measured in pristine conditions (C0). The table reports also the conventional strain limit $\varepsilon_{lim,conv}$, obtained – consistently with CNR DT215 (National Research Council of Italy [CNR] 2020) – as the ratio of σ_{max} and elastic modulus of the fibres. As expected, the effectiveness of the FRGP was in all cases lower than 1, confirming that shear tests, although excluding bond failures, cannot achieve the reference strength of the fibre reinforcements when embedded in inorganic matrices (see also Garbin, Panizza, and Valluzzi

2018). Nonetheless, in the case of steel the exploitation was not lower than 0.8, thus suggesting that steel cords are less sensitive to this type of test. Carbon fibres slipped at values of the exploitation factor comprised between 0.41 and 0.47, while basalt reinforcements failed at values of 0.23 and 0.32, not considering the specimen damaged during handling.

[f]Figure 7 near here[/f]

[t]Table 7 near here[/t]

4.3. Bending tests on single-slice specimens

Unreinforced specimens and bricks with the geopolymer matrix only (without fibres) showed a typical bending failure, located close to the centreline where the moment was maximum. While the bending strength of unreinforced brick slices – about 4.4 MPa in average – was in line with the expected value (see Table 1), those with the geopolymer matrix without fibres failed at lower load levels, about 30% in average. Although this behaviour might appear surprising, it can be straightforwardly explained by considering the different stiffness of fired clay and geopolymer matrix, as discussed in section 5.

Failure of specimens with steel reinforcements, embedded either in geopolymer or epoxy matrix, was generally triggered by near-end debonding, which progressed through inclined cracks converging towards the centreline (Fig. 8a,9a). A similar type of failure was shown also by carbon and basalt FRPs, whereas glass, in all cases, and basalt FRGP broke in tension (Fig. 8c,9b). Carbon FRGP failed due to fibre slippage, consistently with shear tests results. For the sake of comparison, load-movable beam displacement curves are reported in Figure 10, while Figure 11 shows the ratio of average reinforced-to-unreinforced maximum loads. Failure modes and numerical results are listed in Table 8 (where $P_{cr,avg}$ is the average first peak load – not noticed in basalt FRGP specimens – and $P_{max,avg}$ is the average maximum load recorded), together with an estimation of the tensile stress at maximum load ($\sigma_{max,sb}$), calculated via section analysis with the assumption of plain sections and a stress-block $0.8 \cdot x$ deep, being x the neutral axis depth, and its related exploitation coefficient $\eta_{BT,sb}$, which expresses the ratio of tensile

stress and pristine experimental tensile strength and was calculated similarly to the case of η_{ST}. The quantities marked with an apostrophe in Table 8 indicate tensile stresses recalculated by taking into account the contribution of the epoxy layer, approximately 0.8-1.2 mm thick, which appeared not negligible in the case of weaker and less stiff reinforcements, i.e. basalt and glass. The experimental data of Table 7 and Table 8 concerning the FRGPs confirmed the efficiency and consistency of the steel reinforcement and a possible better debonding behaviour of carbon, basalt and glass reinforcements when evaluated via bending tests. This is consistent with the current literature (Calabrese, D'Antino, and Colombi 2021) concerning the influence of the debonding testing methods for FRCMs. The $\eta_{BT,sb}$ and the strength retention factors compares very well for basalt and glass reinforcements, which clearly failed in tension in the bending tests. Lastly, the data of the last two columns of Table 8 evidenced the possible effect of the epoxy matrix, which is provided with a not negligible tensile strength. While this effect is not usually noticeable and then accounted for in larger specimens (Valluzzi et al. 2014), it might provide an non trivial contribution in small scale samples as those herein used.

[f]Figure 8 near here[/f]

[f]Figure 9 near here[/f]

[f]Figure 10 near here[/f]

[f]Figure 11 near here[/f]

[t]Table 8 near here[/t]

4.4. Bending tests on 2-brick specimens

Failure of the 3 unreinforced specimens was always located at the mortar-brick interface (Fig. 12a). They were tested twice, the second time after repair of the failed joint, and showed a remarkably variable resistance comprised between 37 and 129 N, corresponding to a bond strength, calculated as the ratio of maximum bending moment and section modulus, comprised between 0.22 and 0.81 N/mm². The average strength of the weakest joint of each specimen was 0.41 N/mm², while the average of the strongest ones was 0.62 N/mm².

In the case of steel FRGP, failure was triggered by debonding and was eventually due to a shear failure of the brick that started close to the end of the reinforcement (Fig. 12b,c), after a wedge-like cracking of the portion beneath the applied load. Carbon FRGP failed due to slippage and partial rupture of fibres (Fig. 13a,b). Whereas, basalt FRGP broke in tension (Fig. 13c), in all cases in correspondence to the main crack that opened at the mortar-brick interface.

The recorded load-displacement curves are shown in Figure 14 for a general comparison. In fact, it must be noted that the available setup did not allow the use of additional transducers and, consequently, displacements are referred to the movable loading beam.

Results are listed in Table 9, in terms of failure mode, maximum load P_{max} and maximum reinforcement stress $\sigma_{max.sb}$, calculated by means of a section analysis based on the assumption of plain sections and a stress-block $0.8 \cdot x$ high, being x the neutral axis depth. The exploitation coefficient $\eta_{BT,sb}$ was calculated similarly to the case of η_{ST}. Steel-reinforced specimens could not attain a fibre effectiveness close to shear test samples, due to the earlier shear failure of the brick, but in the case of carbon FRGP, which showed a similar failure mode, the exploitation, here comprised between 0.41 and 0.44, was comparable. Conversely, basalt FRGP reached again relatively high values of η_{BT} (0.60 and 0.71) compared to shear tests (damaged sample excluded, cracked by drying shrinkage during the curing phase), probably thanks to the reduced number of strands and to the bending specimen that allowed an evener stress distribution, as mentioned in the previous section.

[f]Figure 12 near here[/f]

[f]Figure 13 near here[/f]

[f]Figure 14 near here[/f]

[t]Table 9 near here[/t]

5. Role of stiffness and strength of the inorganic matrix

In order to shed light on the role of the stiffness and strength of inorganic matrices in the overall behaviour of the reinforced member, a simplified analysis, based on the classical linear

approach for bending of multi-material composite beams, was carried out (Fig. 15a, where b, h are width and height of the cross section, h_b and h_g are height of brick and thickness of geopolymer matrix, x_{na} is the neutral axis depth, ε_{top} and ε_{bot}, σ_{top} and σ_{bot} indicate strains and stresses at top and bottom edge, respectively, C_b, T_b, T_f and T_g are compressive and tensile forces acting on the cross section, with subscripts b, f and g referring to brick, fibres and geopolymer matrix, respectively). The model reproduced the single-brick bending specimen.

The typical assumptions were: perfect bonding of the layers; plane sections remain plane after bending; linear behaviour of materials until the limit tensile stress on the outer edge is reached. For the sake of simplicity, also fibre reinforcements were supposed to be perfectly bonded since the beginning of loading. Realistically, they would be working in tension only after a certain load value, due to their morphological and geometrical features. In fact, the reinforcements are made of strands with only the outer fibrils in contact with the matrix, as also reported in [45]. Lastly, voids in the matrix, related to the embedment of fibre strands, were neglected. Nonetheless, the linear analysis provided useful insight that partly explained the observed behaviour presented in section 4.3.

The model was fed with: measured geometric data, i.e. specimen width (comprised between 31.3 and 32.7 mm), brick depth (54.0-55.0 mm), geopolymer thickness (4.0-5.0 mm), distance of fibre mesh from the bottom edge of the brick (1.0-2.0 mm); mechanical properties from characterization tests, i.e. brick compressive strength (17.7 N/mm²) and Young's modulus in compression ($5.78 \cdot 10^3$ N/mm²), geopolymer tensile strength from splitting tests (4.42 N/mm², assumed to be more representative of the actual behaviour of a relatively thin layer, compared to bending strength) and Young's modulus ($12.7 \cdot 10^3$ N/mm² measured in compression but considered a reliable estimation also in tension, as usually assumed for quasi-brittle materials, e.g. see van Mier 1997); fibre reinforcement strength from characterization (average values in pristine conditions, see Tab. 3) and Young's modulus in tension from datasheets (Tab. 3).

The linear analysis was complemented by a stress-block analysis (see for example Eurocode 2 (European Committee for Standardization 2004) at the same load level (Fig. 15b, where ε_f is the fibres strain, f_c is the compressive strength, λ and η are factors defining the effective height of the compression zone and the effective strength, taken as 0.8 and 1.0 0, respectively, and C_b, T_f are the resultant compression and tension forces), corresponding to the attainment of geopolymer tensile strength at the outer edge and motivated by the experimental observation that the brittle failure of the matrix led to a crack growth through the brick, which generally progressed until it stopped at a new neutral axis related to an equilibrated cracked configuration of the cross-section.

[f]Figure 15 near here[/f]

The analytical results are reported in Table 10. By comparing the data of Table 8 and Table 10, it can be noticed that the experimental and analytical maximum load (P_{max}) of single-brick bending specimens reinforced only with the geopolymer matrix are practically the same. Therefore, the different stiffness of fired clay and geopolymer matrix (Table 1 and Table 2) reasonably triggered the 30% load drop presented in section 4.3. This outcome reemphasized the importance of mechanical compatibility between substrates and inorganic overlays. Moreover, the data underlined the importance of the fibre reinforcements after the cracking of the matrix. In fact, a negligible fibre stress can be inferred from an elastic analysis while the matrix is undamaged, whereas an appreciable stress level for the reinforcements can be derived from a stress block analysis.

[t]Table 10 near here[/t]

6. Summary of exploitation and strength retention factors

Minimum and maximum average strength retention factors, measured via tensile tests on fabric coupons (or cords in the case of steel), are reported in Table 11 with the corresponding conditioning. Exploitation factors η (ratio of tensile stress at maximum load and average tensile

strength of fibres in pristine conditions) calculated for each type of test, i.e. shear, single-brick bending and 2-brick bending tests, are listed as well for a direct comparison. As explained in the previous sections, the nominal tensile stress at maximum load, in the case of bending tests, was estimated through section analysis based on stress-block approach, while that stress was directly obtained by the ratio of applied load and fibres area in the case of shear tests.

The exploitation of steel cords, in bending, was limited by the shear strength of the support material, while the failure of shear tests with 200 mm of bonded length (2 out of 3) was a tensile rupture. Indeed, as general observation, the latter results (0.81 in average) could be explained by considering that shear tests are carried out on reinforcement strips having a width usually greater or equal to 50 mm, representative to a reasonable extent of realistic applications. Consequently, despite the precautions taken, the applied force might have been unevenly distributed among the cords or strands. On the other hand, the reduced width of bending specimens probably promoted a more uniform stress distributions on fibre reinforcements (Calabrese, D'Antino, and Colombi 2021).

Carbon meshes failed in all cases due to slippage inside the matrix, limiting the exploitation to less than 45% of the tensile strength, except for single-brick specimens that allowed a greater ultimate stress.

The exploitation of basalt meshes was approximately comprised between 60-65% in bending, and 26% in shear tests. As already observed (Lignola et al. 2017), the lower strength of basalt reinforcements renders them more sensitive to uneven stress distributions, in comparison to carbon and steel.

Lastly, glass fibres, whose alkali resistant sizing was proved effective, showed a tensile failure in bending at about 100% of tensile strength. However, it can be noted that, compared to epoxy matrix, the performance of G-FRGP in terms of maximum stress was about 80%, while the corresponding comparison for B-FRGP delivers a value of 60%. The difference might be

ascribed to the lack of sizing of basalt fibres and, consequently, to their possibly greater degradation inside the geopolymer matrix, which, however, can reasonably assumed to be lower in comparison to the conditioning of fibres in alkali solution, because of the lower pH value for the geopolymer matrix (Tab. 4) and because the fibres composing the strands are only partially embedded in the matrix, thus possibly not fully in contact with the alkaline medium.

[t]Table 11 near here[/t]

7. Conclusions

The paper presented an assessment of the adhesion and durability properties of FRGPs as strengthening material for masonry structures. The FRGPs were made of an eco-efficient and heat resistant geopolymeric matrix that has a chemical composition and porosity similar to that of soft mud clay bricks simulating a typical historical masonry unit. Therefore, the matrix is an interesting inorganic bonding agent for the implementation of removable and compatible composites suitable, not only for exiting masonry buildings, but also for BH. The four FRGPs studied were reinforced with a unidirectional Ultra High Strength Steel (UHSS) fabric or a bi-directional mesh of non-metallic fibres, either carbon, basalt or alkali-resistant glass, respectively.

The adhesion and mechanical performances of the four FRGPs were investigated by means of local single-lap shear tests on single bricks with a bonded length of either 200 mm or 50mm, and via 3-point bending tests on 1-brick and 2-brick specimens reinforced at the bottom face. The exploitation coefficients derived from the shear and the bending tests were in accordance with the best performances currently delivered by FRCM systems. In addition, FRGPs are provided with an innovative inorganic matrix, which is more sustainable, able to resist to elevated temperatures (greater than 600°C 0) and provided with a chemically compatible composition. Nonetheless, additional studies are necessary to better tailor the stiffness of the matrix, thus improving its mechanical compatibility.

Moreover, further studies are also necessary to investigate the durability of the FRGPs. In fact, the behaviour in alkaline environments simulating those provided by the geopolymeric matrices highlighted the possibility of undesired corrosive outcomes on the fibres, especially when they are un-sized (or they lost part of the sizing) as the basalt mesh used in this research.

The results confirmed the untapped and interesting potential of FRGPs. In particular, the FRGPs reinforced with the carbon mesh and the UHSS fabric showed promising results as potential inorganic composites suitable for strengthening exiting masonry buildings and BH. On the other hand, precautions should be taken with fibre reinforcements sensitive to alkaline environments.

Acknowledgements

Fibres were supplied free of charge by: Fidia s.r.l. (Perugia, Italy) – bidirectional basalt mesh; Kerakoll s.p.a. (Sassuolo, Italy) – unidirectional UHTS steel; BASF CC Italia (Treviso, Italy) – bidirectional carbon and glass mesh. The latter provided pozzolana lime mortar as well. Soft mud clay bricks were provided free of charge by San Marco Terreal Italia (Noale, Italy).

Authors' contribution statement

Enrico Garbin and **Matteo Panizza** contributed equally (co-first authors). **Enrico Garbin:** Conceptualization, Methodology, Investigation, Formal analysis, Writing – Review and Editing, Supervision. **Matteo Panizza:** Methodology, Investigation, Formal analysis, Writing – Original Draft, Writing - Review and Editing, Visualization. **Marco Natali:** Conceptualization, Methodology, Investigation, Supervision. **Gilberto Artioli:** Writing - Review and Editing, Supervision. **Sergio Tamburini:** Conceptualization, Methodology, Investigation, Supervision.

Disclosure Statement

Authors declare that no funding was received for conducting the research, and that there are no relevant financial or non-financial interests, and no other competing interests to disclose.

References

American Concrete Institute. 2013. *ACI 549.4R-13. Guide to Design and Construction of Externally Bonded FRCM Systems for Repair and Strengthening Concrete and Masonry Structures*.

ASTM International 2013. *ASTM E2098/E2098M-13. Standard Test Method for Determining Tensile Breaking Strength of Glass Fiber Reinforcing Mesh for Use in Class PB Exterior Insulation and Finish Systems (EIFS), after Exposure to a Sodium Hydroxide Solution*.

Calabrese A.S., D'Antino T., and Colombi P. 2021. *Experimental and analytical investigation of PBO FRCM-concrete bond behavior using direct and indirect shear test set-ups*. COMPOS STRUCT 264:113672. doi.org/10.1016/j.compstruct.2021.113672

Carabba L., Santandrea M., Carloni C., Manzi S., and Bignozzi M.C. 2017. *Steel fiber reinforced geopolymer matrix (S-FRGM) composites applied to reinforced concrete structures for strengthening applications: A preliminary study*. COMPOS PART B-ENG 128:83 90. doi:10.1016/j.compositesb.2017.07.007

Ceroni F. and Salzano P. 2018. *Design provisions for FRCM systems bonded to concrete and masonry elements*. COMPOS PART B-ENG 143:230-242. doi:10.1016/j.compositesb.2018.01.033

Coletti C., Cultrone G., Maritan L., and Mazzoli C. 2016. *How to face the new industrial challenge of compatible, sustainable brick production: Study of various types of commercially available bricks*. APPL CLAY SCI 124-125:219-226. doi:10.1016/j.clay.2016.02.014

de Felice G., De Santis S., Garmendia L., Ghiassi G., Larrinaga P., Lourenço P.B., Oliveira D.V., Paolacci F., and Papanicolaou C.G. 2014. *Mortar-based systems for externally bonded strengthening of masonry*. MATER STRUCT 47(12):2021-2037. doi:10.1617/s11527-014-0360-1

Dhand V., Mittal G., Rhee K.Y., and Hui D. 2015. *A short review on basalt fiber reinforced polymer composites*. COMPOS PART B-ENG 73:166-180. doi:10.1016/j.compositesb.2014.12.011

European Committee for Standardization. 2004. *EN 1992-1-1. Eurocode 2 – Design of concrete structures - Part 1-1: General rules and rules for buildings*.

European Committee for Standardization. 2005. *EN 1996-1-1 Eurocode 6 – Design of masonry structures. General rules for reinforced and unreinforced masonry structures*.

Ferone C., Colangelo F., Roviello G., Asprone D., Menna D., Balsamo A., Prota A., Cioffi R., and Manfredi G. (2013). *Application-oriented chemical optimization of a metakaolin based geopolymer*. MATERIALS 6(5):1920-1939. doi:10.3390/ma6051920

Garbin E. 2008. *Characterization of bed joint reinforced brick masonry subjected to compression*. Ph.D. Thesis, University of Trento, Trento, Italy.

Garbin E., Panizza M., and Valluzzi M. R. 2018. *Experimental Characterization of Glass and Carbon FRCMs for Masonry Retrofitting*. ACI Special Publication, 324:3.1-3.20.

Garbin E., Panizza M., Valluzzi M.R., Nardon F., Tamburini S., Favaro M., and Magro A. 2014. *Characterization of Fibre Reinforced Geopolymers as structural strengthening material for historical brick masonry*. in: Proc. of 9th Int. Masonry Conference, Guimarães, Portugal, 7-9 July, 8 pp.

Garmendia L., Marcos I., Garbin E., and Valluzzi M.R. 2014. *Strengthening of Masonry Arches with Textile-Reinforced Mortar: Experimental Behaviour and Analytical Approaches*. MATER STRUCT 47(12):2067-2080. doi:10.1617/s11527-014-0339-y

Girardello, P. 2013. *Rinforzo di volte in muratura con materiali compositi innovativi*. Ph.D. Thesis, University of Brescia and University of Padova, Italy. *In Italian*.

Gkournelos P.D., Azdejković L.D., and Triantafillou T.C. (2022). *Innovative and Eco-friendly Solutions for the Seismic Retrofitting of Natural Stone Masonry Walls with Textile Reinforced Mortar: In- and Out-of-Plane Behavior*. J COMPOS CONSTR 26(1):04021061. doi.org/10.1061/(ASCE)CC.1943-5614.0001173

Hollaway L.C. 2010. *A Review of the Present and Future Utilisation of FRP Composites in the Civil Infrastructure with Reference to Their Important In-service Properties*. CONSTR BUILD MATER 24(12):2419-2445. doi:10.1016/j.conbuildmat.2010.04.062

Katakalos K., and Papakonstantinou C.G. (2009). *Fatigue of reinforced concrete beams strengthened with steel-reinforced inorganic polymers*. J COMPOS CONSTR 13(2):103-112. doi:10.1061/(ASCE)1090-0268(2009)13:2(103)

Kouris L.A.S., and Triantafillou T.C. 2018. *State-of-the-art on strengthening of masonry structures with textile reinforced mortar (TRM)*. CONSTR BUILD MATER 188:1221-1233. doi:10.1016/j.conbuildmat.2018.08.039

Kurz S., and Balaguru P.N. 2001. *Comparison of Inorganic and Organic Matrices for Strengthening of RC Beams with Carbon Sheets*. J STRUCT ENG 127(1):35-42. doi:10.1061/(ASCE)0733-9445(2001)127:1(35)

Lignola G.P., Caggegi C., Ceroni F., De Santis S., Krajewski P., Lourenço P.B., Morganti M., Papanicolaou C., Pellegrino C., Prota A., et al. 2017. *Performance Assessment of Basalt FRCM for Retrofit Applications on Masonry*. COMPOS PART B-ENG 128:1-18. doi.org/10.1016/j.compositesb.2017.05.003

Menna C., Asprone D., Ferone C., Colangelo F., Balsamo A., Prota A., Cioffi R., and Manfredi G. (2013). *Use of geopolymers for composite external reinforcement of RC members*. COMPOS PART B-ENG 45(1):1667-1676. doi:10.1016/j.compositesb.2012.09.019

Meriggi P., de Felice G., and De Santis S. (2020). *Design of the out-of-plane strengthening of masonry walls with fabric reinforced cementitious matrix composites*. CONSTR BUILD MATER 240:117946. doi:10.1016/j.conbuildmat.2019.117946

Modena C., Valluzzi M.R., da Porto F., and Casarin F. 2011. *Structural Aspects of the Conservation of Historic Masonry Constructions in Seismic Areas: Remedial Measures and Emergency Actions*. INT J ARCHIT HERIT 5(4-5):539-558. doi:10.1080/15583058.2011.569632

National Research Council of Italy. 2013. *CNR DT 200R1/2013. Guide for the Design and Construction of Externally Bonded FRP Systems for Strengthening Existing Structures*.

National Research Council of Italy. 2020. *CNR DT 215/2018. Guide for the Design and Construction of Externally Bonded Fibre Reinforced Inorganic Matrix Systems for Strengthening Existing Structures*.

Pacheco-Torgal F., and Jalali S. 2011. *Eco-Efficient Construction and Building Materials*. Woodhead Publishing Ltd. ISBN 978-0-85709-767-5.

Panizza M., Garbin E., Valluzzi M.R. and Modena, C. 2012. *Experimental investigation on bond of FRP/SRP applied to masonry prisms*. In Proc. of 6th Int. Conf. on FRP composites in Civil Engineering – CICE2012, Rome, Italy, 13-15 June. G. Monti ed.

Papakonstantinou C.G., and Katakalos K. (2009). *Flexural behavior of reinforced concrete beams strengthened with a hybrid inorganic matrix-steel fibre retrofit system*. STRUCT ENG MECH 31(5):567-585. doi:10.12989/sem.2009.31.5.567

Papanicolaou C.G., Triantafillou T.C., Karlos K., and Papathanasiou M. 2007. *Textile-Reinforced Mortar (TRM) Versus FRP as Strengthening Material of URM Walls: In-plane Cyclic Loading*. MATER STRUCT 40(10):1081-1097. doi:10.1617/s11527-006-9207-8

Papanicolaou C.G., Triantafillou T.C., Papathanasiou M., and Karlos K. 2008. *Textile Reinforced Mortar (TRM) Versus FRP as Strengthening Material of URM Walls: Out-of-plane Cyclic Loading*. MATER STRUCT 41(1):143-157. doi:10.1617/s11527-007-9226-0

Provis L., and van Deventer J.S.J. (2009). *Geopolymers: Structure, processing and industrial applications*. Woodhead Publishing Ltd. ISBN 978-1-84569-449-4.

Shaikh F.U.A. (2013). *Review of mechanical properties of short fibre reinforced geopolymer composites*. CONSTR BUILD MATER 43:37 49. doi:10.1016/j.conbuildmat.2013.01.026

Shrive N.G. 2006. *The Use of Fibre Reinforced Polymers to Improve Seismic Resistance of Masonry*. CONSTR BUILD MATER 20(4):269-277. doi:10.1016/j.conbuildmat.2005.08.030

Tamburini S., Natali M., Garbin E., Panizza M., Favaro, and Valluzzi M.R. 2017. *Geopolymer matrix for fibre reinforced composites aimed at strengthening masonry structures*. CONSTR BUILD MATER 141:542-552. doi:10.1016/j.conbuildmat.2017.03.017

Tamburini S., Natali M., Garbin E., Valluzzi M.R., and Artioli G. 2015. *Comparison of fibres in geopolymer matrix for structural reinforcement of masonry (FRGP): Compatibility, reactivity, durability*. In: ECI Conference on Geopolymers. The route to eliminate waste and emissions in ceramic and cement manufacturing, Schloss Hernstein (Austria), 24-29 May, 4 pp.

Tedeschi C., Kwiecien A., Valluzzi M.R., Zajac B., Garbin E., and Binda L. 2014. *Effect of thermal ageing and salt decay on bond between FRP and masonry*. MATER STRUCT 47(12):2051-2065. doi:10.1617/s11527-014-0448-7

Tomaževič M. 2011. *Seismic Resistance of Masonry Buildings in Historic Urban and Rural Nuclei: Lessons Learned in Slovenia*. INT J ARCHIT HERIT 5(4-5):436-465. doi:10.1080/15583051003792898

Toutanji H., and Deng Y. 2007. *Comparison between organic and inorganic matrices for RC beams strengthened with carbon fiber sheets*, J COMPOS CONSTR 11(5):507-513. doi:10.1061/(ASCE)1090-0268(2007)11:5(507)

Triantafillou T. 2016. *Textile Fibre Composites in Civil Engineering*. Woodhead Publishing. ISBN 978-1-78242-446-8. eISBN 978-1-78242-469-7. doi:10.1016/C2014-0-01415-3

Triantafillou T.C. 1998. *Strengthening of Masonry Structures Using Epoxy-Bonded FRP Laminates*. J COMPOS CONSTR 2(2):96-104. doi:10.1061/(ASCE)1090-0268(1998)2:2(96)

Valluzzi M.R., da Porto F., Garbin E., and Panizza M. 2014. *Out-of-plane behaviour of infill masonry panels strengthened with composite materials*. MATER STRUCT 47:2131-2145. doi.org/10.1617/s11527-014-0384-6

Valluzzi M.R., Modena C., and de Felice G. 2014. *Current Practice and Open Issues in Strengthening Historical Buildings with Composites*. MATER STRUCT 47(12):1971-1985. doi:10.1617/s11527-014-0359-7

Valluzzi M.R., Oliveira D.V., Caratelli A., Castori G., Corradi M., de Felice G., Garbin E., Garcia D., Garmendia L., Grande E. et al. 2012. *Round Robin Test for composite-to-brick shear bond characterization*. MATER STRUCT 45:1761-1791. doi.org/10.1617/s11527-012-9883-5

van Mier J.G.M. 1997. *Fracture processes of concrete: Assessment of Material Parameters for Fracture Models*. London, UK, CRC press. ISBN 0-8493-9123-7

Vickers L., van Riessen A., and Rickard W.D.A. 2015. *Fire-resistant Geopolymers: Role of fibres and fillers to enhance thermal properties*. Springer, Singapore. ISBN 978-981-287-310-1. eISBN 978-981-287-311-8. doi:10.1007/978-981-287-311-8

Welter M., Schmücker M., and MacKenzie K.J.D. 2014. *Evolution of the fibre-matrix interactions in basalt-fibre-reinforced geopolymer-matrix composites after heating*. J CERAM SCI TECHNOL 6(1):17-24. doi:10.4416/JCST2014-00034

Zhu M., Zhu J.H., Ueda T., Matsumoto K., and Su M. 2021. *Bond behavior of carbon fabric reinforced cementitious matrix (FRCM) composites considering matrix impregnation*. COMPOS STRUCT 262:113350. doi.org/10.1016/j.compstruct.2020.113350

Figure 1. Samples of steel (a) and basalt (b) reinforcement for tensile tests, and a coupon ready for testing (c)

Figure 2. Sketch of shear test specimens, with sizes in mm (a); a steel FRGP ready for testing (b); and sample with bonded length L_b = 50 mm

Figure 3. Sketch of 2-brick (top) and single-brick bending specimens, with sizes in mm (a); and a reinforced 2-slice specimen ready for testing (b)

Figure 4. Weight loss (a) and tensile strength retention (b) measured on conditioned fibres

Figure 5. Shear tests on steel and carbon FRGP with L_b = 200 mm: steel tensile failure (a); the only partial debonding (b); diffuse cracking of the matrix embedding carbon mesh, highlighted in red (c); and slippage of carbon strands (d)

Figure 6. Tensile failure of basalt fibres in samples with either L_b = 200 mm (a), or L_b = 50 mm (b); brick failure of steel FRGP with L_b = 50 mm (c)

Figure 7. Measured load–loaded end displacement curves for shear tests (L_b stands for bonded length)

Figure 8. Typical failures of steel (a), carbon (b) and basalt/glass (c) reinforced geopolymers

Figure 9. Typical failure of FRP reinforced brick specimens: debonding/shear (a) and fibre tensile rupture (b)

Figure 10. Measured load-beam displacement for bending tests on single brick specimens (GP and EP indicate either geopolymer or epoxy matrix, respectively)

Figure 11. Performance of geopolymer (GP) and epoxy (EP) matrices coupled to fibre fabrics, compared to unreinforced bricks (URM) in terms of average maximum load. Error bars indicate ± 1 standard deviation normalized to $P_{max,URM}$

Figure 12. Failure modes of bending tests: (a) joint failure of unreinforced specimens; (b) brick shear failure and (c) detail of the wedge isolated by inclined cracks, in case of steel FRPG

Figure 13. Failure modes of bending tests: (a) slippage with partial rupture and (b) detail of cracking in case of carbon FRPG; (c) tensile failure of basalt mesh

Figure 14. Measured load–movable beam displacement curves for jointed brick specimens

Figure 15. Sketch for the uncracked cross section in case of linear analysis (a), and the cracked cross section in case of stress-block analysis (b)

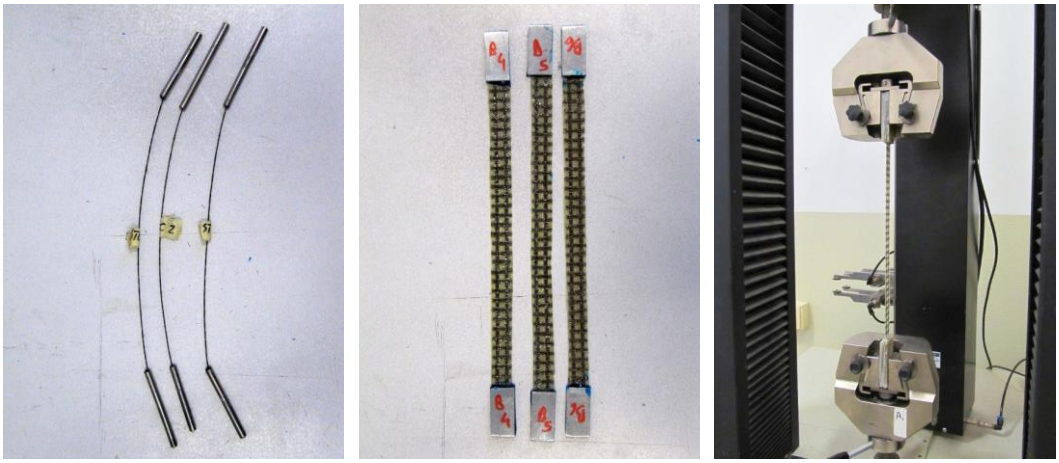

(a) (b) (c)

Figure 1. Samples of steel (a) and basalt (b) reinforcement for tensile tests, and a coupon ready for testing (c)

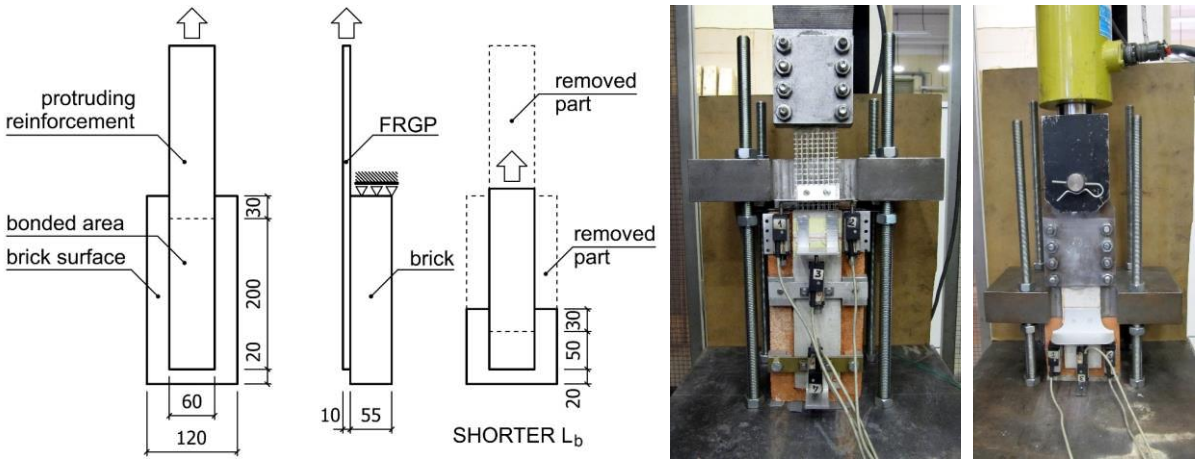

(a) (b) (c)

Figure 2. Sketch of shear test specimens, with sizes in mm (a); a steel FRGP ready for testing (b); and sample with bonded length L_b = 50 mm

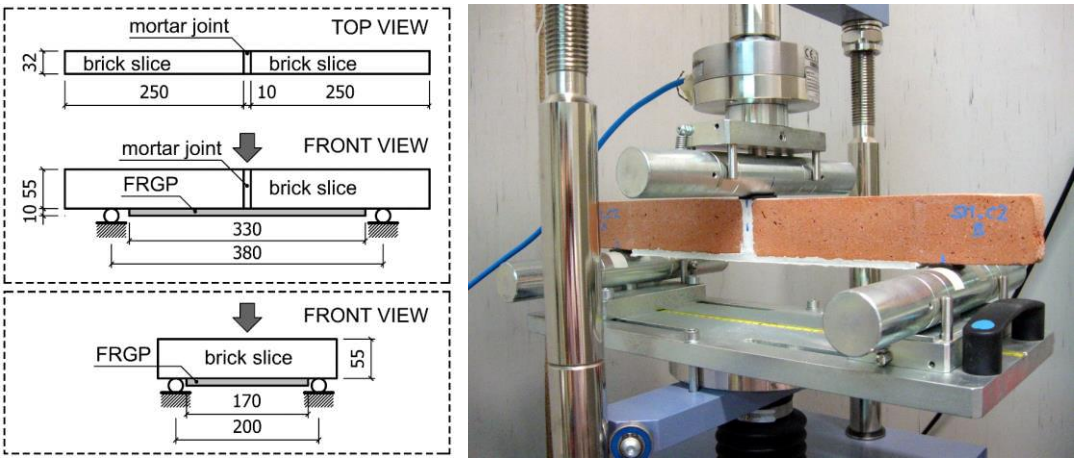

(a) (b)

Figure 3. Sketch of 2-brick (top) and single-brick bending specimens, with sizes in mm (a); and a reinforced 2-slice specimen ready for testing (b)

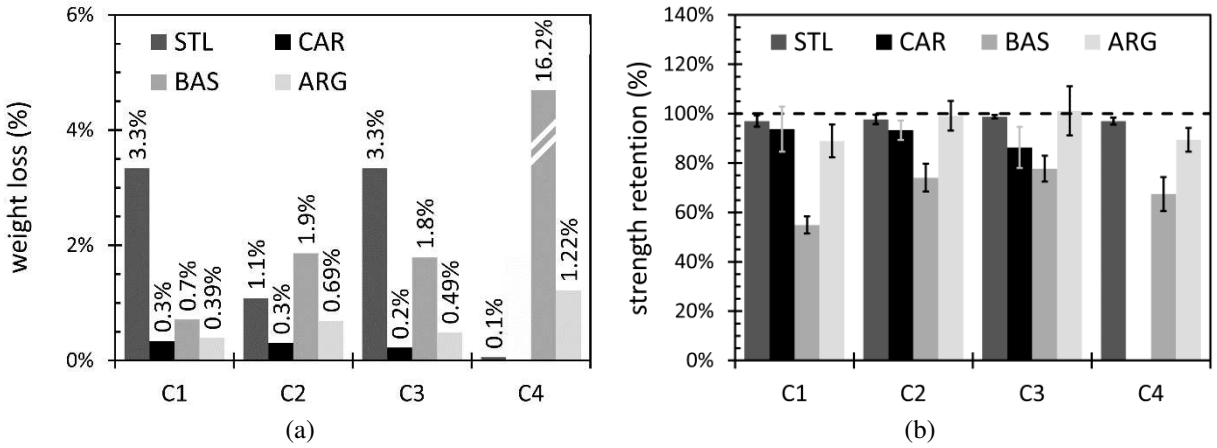

1 **Figure 4. Weight loss (a) and tensile strength retention (b) measured on conditioned fibres**

2

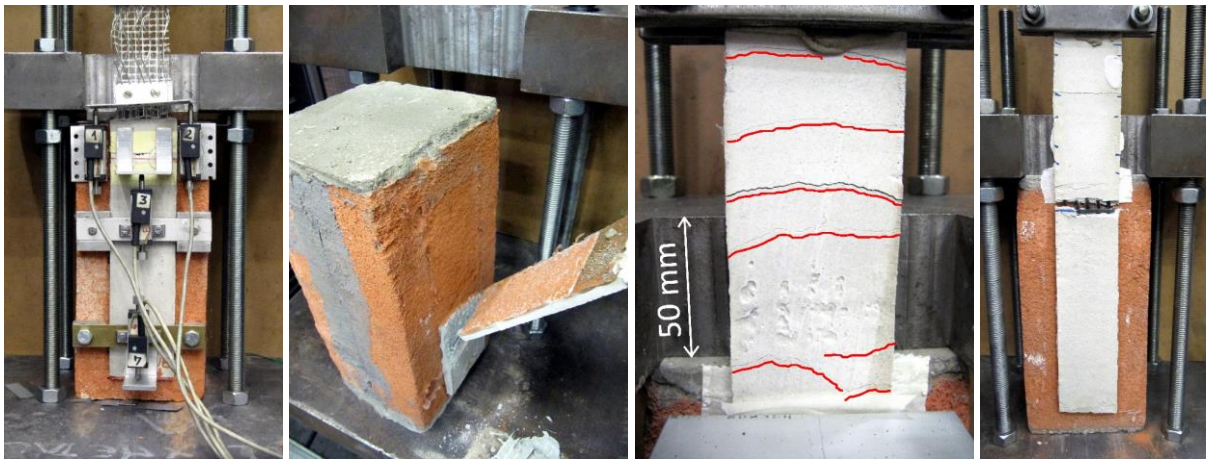

(a) (b) (c) (d)

Figure 5. Shear tests on steel and carbon FRGP with L_b = 200 mm: steel tensile failure (a); the only partial debonding (b); diffuse cracking of the matrix embedding carbon mesh, highlighted in red (c); and slippage of carbon strands (d)

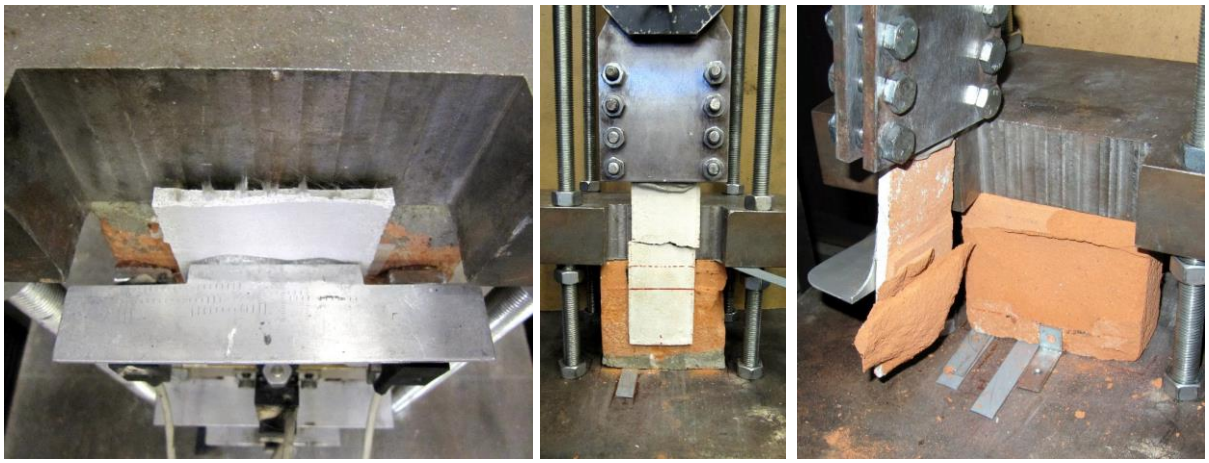

(a) (b) (c)

Figure 6. Tensile failure of basalt fibres in samples with either L_b = 200 mm (a), or L_b = 50 mm (b); brick failure of steel FRGP with L_b = 50 mm (c)

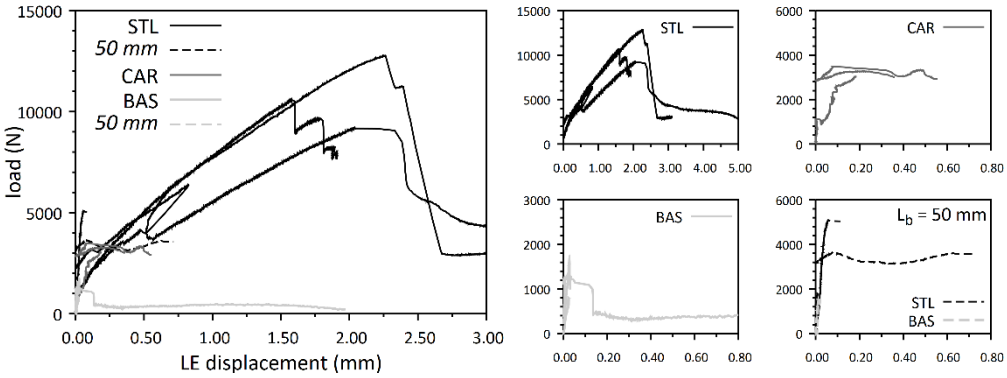

Figure 7. Measured load–loaded end displacement curves for shear tests (*L_b* stands for bonded length)

(a) (b) (c)

Figure 8. Typical failures of steel (a), carbon (b) and basalt/glass (c) reinforced geopolymers

(a) (b)

Figure 9. Typical failure of FRP reinforced brick specimens: debonding/shear (a) and fibre tensile rupture (b)

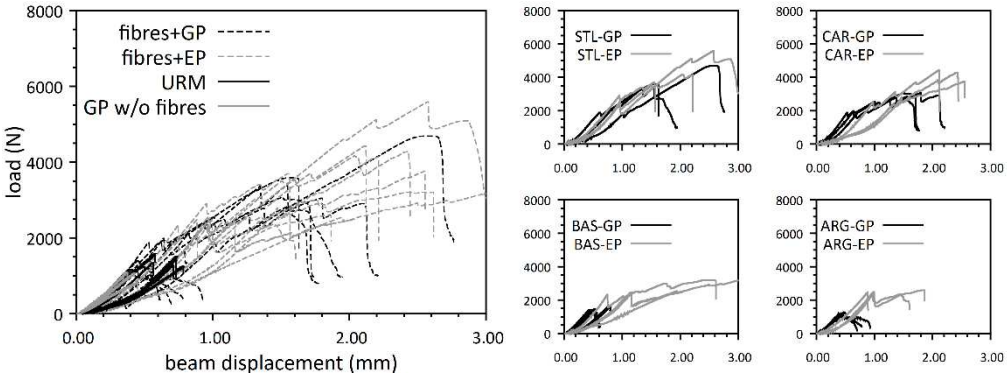

Figure 10. Measured load-beam displacement for bending tests on single brick specimens (GP and EP indicate either geopolymer or epoxy matrix, respectively)

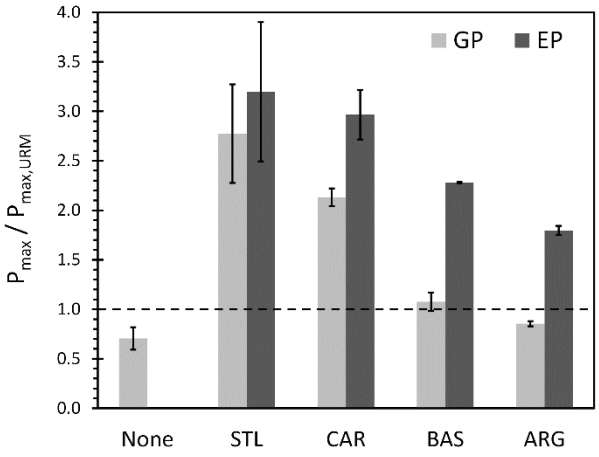

Figure 11. Performance of geopolymer (GP) and epoxy (EP) matrices coupled to fibre fabrics, compared to unreinforced bricks (URM) in terms of average maximum load. Error bars indicate ± 1 standard deviation normalized to $P_{max,URM}$

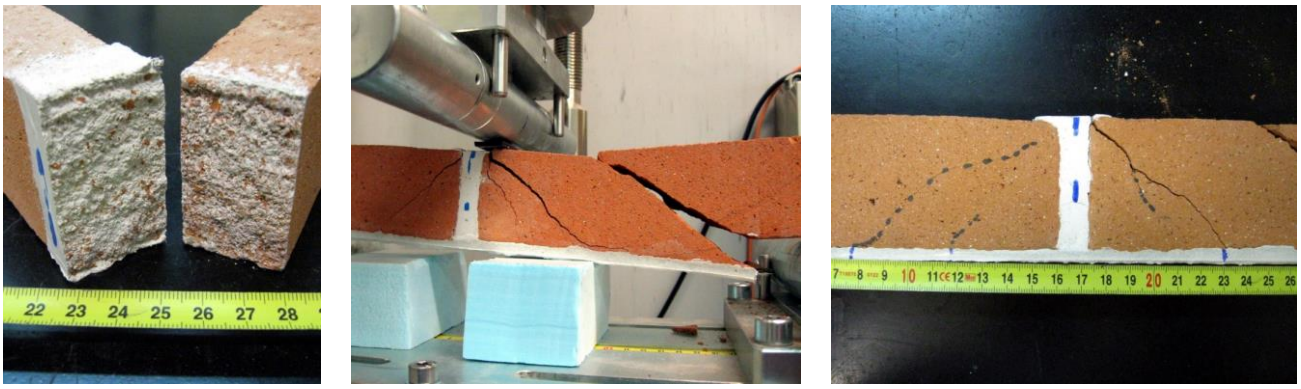

(a) (b) (c)

Figure 12. Failure modes of bending tests: (a) joint failure of unreinforced specimens; (b) brick shear failure and (c) detail of the wedge isolated by inclined cracks, in case of steel FRPG

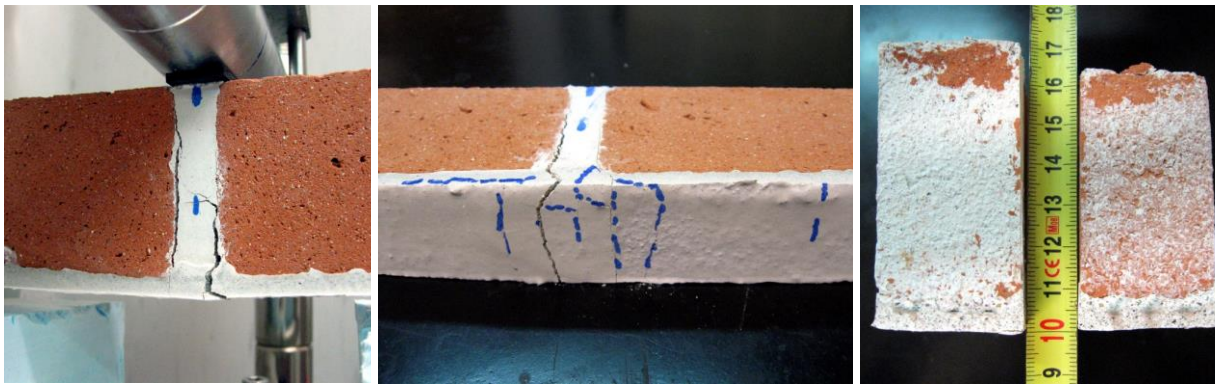

(a) (b) (c)

Figure 13. Failure modes of bending tests: (a) slippage with partial rupture and (b) detail of cracking in case of carbon FRPG; (c) tensile failure of basalt mesh

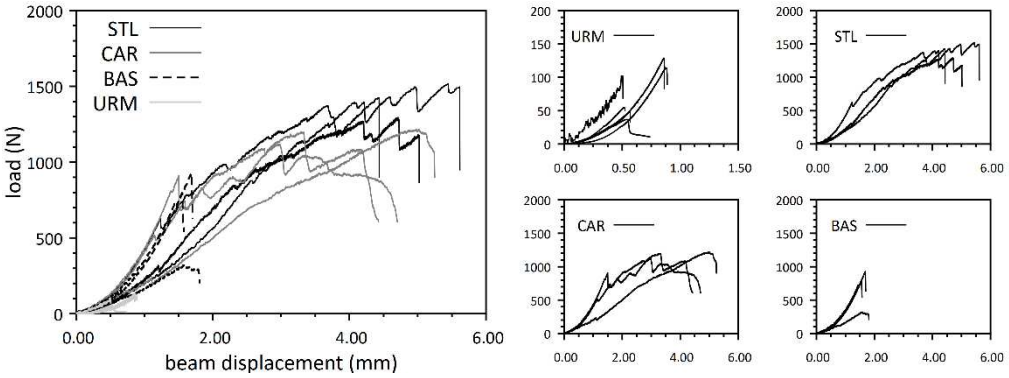

Figure 14. Measured load–movable beam displacement curves for jointed brick specimens

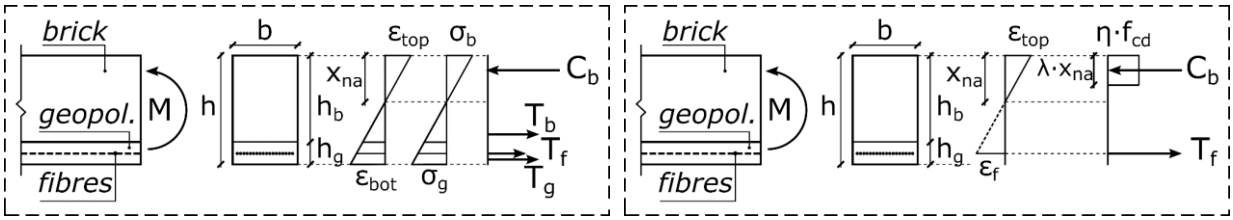

(a) (b)

Figure 15. Sketch for the uncracked cross section in case of linear analysis (a), and the cracked cross section in case of stress-block analysis (b)

Table 1. Properties of soft mud clay bricks and natural hydraulic lime mortar (coefficient of variation in brackets).

Material	ρ_{app} kg/m³	OP %	f_c N/mm²	f_b N/mm²	f_{sp} N/mm²	E_c N/mm²
Bricks	$1.60 \cdot 10^3$ (0.5%)	38.0 (1.9%)	17.7 (6.2%)	4.43 (10.3%)	2.99 (11.2%)	$5.76 \cdot 10^3$ (5.2%)
Lime mortar	$1.81 \cdot 10^3$ (0.2%)	34.1 (2.6%)	14.7 (6.3%)	2.92 (14.5%)	2.03 (3.1%)	$9.06 \cdot 10^3$ (2.8%)

1 **Table 2. Mean properties of geopolymer matrix (coefficient of variation in brackets).**

ρ_{app} kg/m³	OP %	f_c N/mm²	f_b N/mm²	f_{sp} N/mm²	E_c N/mm²
$1.91 \cdot 10^3$ (1.1%)	27.0% (0.6%)	42.05 (12.4%)	7.15 (14.2%)	4.42 (7.1%)	$12.7 \cdot 10^3$ (2.1%)

2
3

Table 3. Main properties of fibre reinforcements.

Reinforcement	Code	$\rho_{s,ds}$ g/m²	$t_{ef,ds}$ mm	$t_{ef,cal}$ mm	E_{ds} N/mm²	$f_{tk,ds}$ N/mm²	$f_{t,avg,exp}$ N/mm²	$f_{tk,exp}$ N/mm²
UHTS Steel	STL	660*	0.075	–	$190 \cdot 10^3$	2820	3125 (0.5%)	3094
Carbon	CAR	200	0.048†	0.056	$230 \cdot 10^3$	2500	2854 (7.9%)	2388
Basalt	BAS	300	0.053	–	$90 \cdot 10^3$	1735	1845 (3.2%)	1729
A.R. glass	ARG	220	0.036†	0.042	$65 \cdot 10^3$	1300	1260 (4.7%)	1153

* *thermal welding and support mesh included*

† *provided by the current datasheet but non disclosed in the former one*

Table 4. pH values measured on the alkali solutions and on two batches of geopolymer matrix.

Substance	initial value*	final value	average
Solution C1	13.62	13.55	13.59
Solution C2	13.21	12.95	13.08
Solution C3	13.24	13.07	13.16
Solution C4	13.58	13.36	13.47
Geopolymer	10.54	10.16	

** for the alkali solutions, initial and final values refer to before and after the conditioning of fibres, while for the geopolymer matrix they refer to the hardened geopolymer respectively measured at early age (24-48 h of curing) and after approximately 1 year (average of 2 samples)*

Table 5. Tensile strength of fibres after conditioning in alkali solutions (CoV in brackets).

Fibre	C1		C2		C3		C4	
	$f_{t,avg}$	$f_{t,k}$	$f_{t,avg}$	$f_{t,k}$	$f_{t,avg}$	$f_{t,k}$	$f_{t,avg}$	$f_{t,k}$
STL	3033 (2.4%)	2877	3053 (1.9%)	2924	3086 (0.7%)	3041	3031 (1.4%)	2936
CAR	2675 (9.7%)	1991	2663 (4.3%)	2364	2464 (9.7%)	1838	–	–
BAS	1013 (6.3%)	864	1367 (7.5%)	1126	1434 (6.8%)	1221	1245 (10.2%)	949
ARG	1121 (7.5%)	1022	1249 (7.2%)	1144	1275 (9.8%)	945	1126 (5.4%)	966

Table 6. Experimentally derived strength retention factors, via mean (avg) and characteristic (k) strength values.

Fibre	C1		C2		C3		C4	
	avg	k	avg	k	avg	k	avg	k
STL	0.970	0.930	0.977	0.945	0.988	0.983	0.970	0.949
CAR	0.937	0.834	0.990	0.933	0.863	0.770	–	–
BAS	0.549	0.500	0.741	0.651	0.777	0.706	0.675	0.549
ARG	0.890	0.887	0.894	0.838	1.012	0.820	0.991	0.992

Table 7. Experimental results of shear tests.

Fibre type	L_b mm		Failure mode	P_{max} N	σ_{max} N/mm²	η_{ST}	$\varepsilon_{lim,conv}$ %
Steel	200	#1	tensile failure	12764	2966	0.95	1.56%
		#2	debonding	9214	2141	0.69	1.13%
		#3	tensile failure	10678	2481	0.79	1.31%
Steel	50	*#1*	debonding / brick failure	5077	1180	0.38	0.62%
		#3	debonding / brick failure	3640	846	0.27	0.45%
Carbon	200	#1	fibre slippage / tensile fail.	3271	1140	0.44	0.50%
		#2	fibre slippage / tensile fail.	3480	1213	0.47	0.53%
		#3	fibre slippage / tensile fail.	3030	1057	0.41	0.46%
Basalt	200	#1	*tensile failure **	*804**	*271**	*0.15**	*0.30%**
		#2	tensile failure	1285	433	0.23	0.48%
		#3	tensile failure	1737	585	0.32	0.65%
Basalt	50	*#1*	tensile failure	1562	526	0.29	0.58%
		#3	tensile failure	1271	428	0.23	0.48%

** specimen damaged during handling before the test*

Table 8. Results of single-slice bending tests (average of 3 tests – 6 for unreinforced specimens).

Fibre type	Matrix	Failure mode	$P_{cr,avg}$ N	$P_{max,avg}$ N	$\sigma_{max,sb}$ N/mm²	$\eta_{BT,sb}$	$\sigma'_{max,sb}$ N/mm²	$\eta'_{BT,sb,EP}$
none	*none*	bending	— —	1403 (9.3%)				
none	GP	bending	— —	989 (16.2%)				
steel	GP	debond. / brick fail.	1950 (6.8%)	3891 (18.0%)	2577 (18.0%)	0.80		
carbon	GP	fibre slippage	1876 (6.4%)	2989 (4.2%)	1648 (4.4%)	0.64		
basalt	GP	fibre tensile failure	— —	1508 (8.6%)	1120 (8.9%)	0.61		
glass	GP	fibre tensile failure	961 (18.5%)	1197 (3.1%)	1195 (3.1%)	1.00		
steel	EP	debonding	2623 (10.0%)	4485 (22.0%)	3052 (24.3%)	0.94	2756	0.85
carbon	EP	debonding	2589 (7.1%)	4160 (8.4%)	2361 (9.0%)	0.92	2155	0.84
basalt	EP	debonding	2661 (11.0%)	3199* (0.4%)	2424* (3.0%)	1.31*	1832*	0.99*
glass	EP	fibre tensile failure	2479 (0.5%)	2520 (2.5%)	2590 (2.6%)	2.17	1483	1.24

** average of 2 specimens, test #1 was stopped at 2500 N (after P_{cr}) due to an issue with the load cell*

Table 9. Experimental results of 2-slice bending tests.

Fibre type		Failure mode	P_{max} N	$\sigma_{max,sb}$ N/mm²	*avg. (CoV)*	$\eta_{BT,sb}$	*avg.*	ε_{conv} %	*avg.*
Steel	#1	brick failure	1289	1591	1770 (9.4%)	0.49	0.55	0.84	0.93
	#2	brick failure	1425	1799		0.56		0.95	
	#3	brick failure	1515	1919		0.59		1.01	
Carbon	#1	fibre slippage	1218	1257	1228 (4.1%)	0.44	0.43	0.55	0.53
	#2	fibre slippage	1119	1170		0.41		0.51	
	#3	fibre slipp. / brick fail.	1199	1258		0.44		0.55	
Basalt	#1	*tensile failure **	*321**	*434**	1208 (11.0%)	*0.24**	0.65	*0.48**	1.34
	#2	tensile failure	798	1114		0.60		1.24	
	#3	tensile failure	927	1302		0.71		1.45	

** mortar joint cracked before the test, probably due to drying shrinkage of the FRGP*

1 **Table 10. Results of the section analyses for single-brick bending specimens.**

Parameter	unit	GP only	S-FRPG	C-FRPG	B-FRPG	G-FRPG
neutral axis depth (elastic)	mm	32.0	32.1	33.2	32.2	32.6
max bending moment per unit width	N·mm/mm	1568	1594	1746	1605	1636
related applied load	N	988	1023	1101	1012	1016
tensile force on geopolymer	N	642	533	641	641	633
tensile force on fibre reinforcement	N		86	117	34	18
neutral axis depth (stress-block)	mm		2.0	2.2	2.1	2.1
tensile force on fibre reinforcement	N		935	1014	948	935
related fibre stress / tensile strength	%		20.0%	22.8%	40.4%	84.9%

2
3

Table 11. Average measured strength retention and exploitation factors.

Fibre type	Strength retention factors		Exploitation factors		
	MIN	MAX	η_{ST} – *shear tests**	η_{BT} – *single-brick bending tests†*	η_{BT} – *2-brick bend. tests‡*
Steel	0.970 (C4)	0.988 (C3)	0.809	0.795	0.546
Carbon	0.863 (C3)	1.086 (C4)	0.441	0.639	0.430
Basalt	0.549 (C1)	0.777 (C3)	0.267	0.607	0.655
Glass	0.890 (C1)	1.012 (C3)		1.003	

** STL: 200 mm only, prevalence of tensile failure; CAR: slippage/tensile failure of fibres; BAS: 200 and 50 mm, tensile failure*

† STL: debonding/brick failure; CAR: slippage of fibres; BAS: tensile failure; ARG: tensile failure

‡ STL: brick failure; CAR: slippage of fibres; BAS: tensile failure